Reply to the reviewer's comments on the revised Manuscript No. AMT-2017-119 by K. Gierens, K. Eleftheratos, and R. Sausen

Remarks

We would like to thank the Editor for sending the revised version to the reviewer. In the first review some comments were unfortunately misunderstood and we are grateful for the clarifications in the 2nd review, which makes it much more easy to respond appropriately.

Questions by the referee are reprinted in the following in *italic font* for convenience. Our replies are in upright font.

New changes to the 2nd revised manuscript are marked in blue colour. The red marks of the first revision are retained. In addition, we provide a supplement with material on actual weighting functions and information on the use of weighting functions and Jacobians.

Reply to the reviewer

2.1/General

A clarification: There are two relevant components of physics here: atmospheric physics and instrument physics. To me, a physics-based calibration means a calibration that takes the instrument physics into account. To the authors, it means a calibration that takes the atmospheric physics into account, as radiative transfer indeed does. The authors take into account explicitly atmospheric physics, but not instrument physics. I think this needs to be clarified early in the paper, including in the abstract, as some readers may (like me) expect an explicit consideration of instrument physics when it says "based on physical considerations", such as some instrument calibration papers have.

Indeed, a full treatment of the problems at hand needs consideration of both the atmospheric physics and the instrument physics part. Thanks to the clarification we understand now the referee's concern of the word "physics" in the title. We agree to add a sentence in the abstract and introduction stating that we only treat the atmospheric physics part of the problem, assuming that the instrument physics (calibration etc.) did not change during the period of common operation of N14 and N15.

I have noticed that the authors reason in several locations, in replies to comments of both reviewers, draw conclusions from the expectation that otherwise the "the data could not be used in any meaningful way.". I find this reasoning problematic. HIRS is an operational instrument and was designed for weather forecasting. Producing climate data records is a climate application. It is possible that instrument behaviour poses problems for climate but not for weather applications. Therefore, the conclusion "HIRS is used, thus it can't be too bad" is not generally applicable. A changing SRF is an example: 4D-VAR / reanalysis might cope with that through semi-automatic bias correction, but it may pose a problem for climate data record development. Although I don't expect that the authors undertake a full physics based recalibration/intercalibration/harmonisation of HIRS as this is a massive undertaking, I appreciate that the authors now state explicitly in the conclusions that they assume spectral and radiometric calibration is constant over the study period. This assumption is only stated in the very final line of the conclusion; this should additionally be stated early in the paper.

We also agree that weather and climate applications of satellite data are different things and that a "homogeneous" 30+ year time series is not required for assimilation into weather forecast

models. There is no need to expand on this discussion, since it does refer only to our reply, not to the manuscript text.

The statement, that spectral and radiometric calibration had to be assumed as unchanging appears together with the "physics" comment in the new sentence which we inserted in the abstract and the introduction.

2.11/Section 4.2

I assume those are 1-sigma uncertainty estimates like earlier uncertainties (it would not hurt to state that here, too). That means (-0.5 ± 1.1) *K is a good result, and* (-0.8 ± 0.5) *K is still consistent. However,* (-1.2 ± 0.4) *K is statistically significantly different from 0, which means there is some residual that the regression fails to correct for. There are good reasons why this is the case, but this should be explicitly noted.*

Yes, the quoted uncertainties are 1-sigma uncertainties and this will be noted.

We note also that it turned out necessary to retain the full precision of the bilinear regression coefficients to reproduce the figures exactly. Using the full precision changes the mean and standard deviation of regressand minus regressor
from (-0.8 ± 0.5) K to (0.0 ± 0.6) K for Lindenberg,
from (-0.5 ± 1.1) K to (0.3 ± 1.3) K for Sodankylä,
from (-1.2 ± 0.4) K to (-0.4 ± 1.3) K for Manus.

We admit that there is some residual that the regression using T_{11} does not correct for. It is not really surprising, and we have noted that already in section 4.1 writing "One additional piece of information is clearly insufficient to capture all this variability". For clarity, we add a sentence into the section 4.2.

2.12/2.13/Section 5.1

I understand the author's reasoning, and a generic weighting function is useful for the states purposes. But specific weighting functions for the relevant atmospheric conditions are relevant to interpret the differences in brightness temperatures. As your reply shows, even at Lindenberg with its relatively mild winters, NOAA-14 observes the ground in some cases (which, btw, is not at 0m at either Lindenberg or Sodankylä, I don't know for Manus, so the Jacobian should stop above 0m). I would expect that to be common in the Sodankylä winter, which is why I asked for a Sodankylä winter Jacobian, which unfortunately the authors have not provided either in the reply or in the revised paper.

At the end of this reply we have plotted two pairs of weighting functions for winter profiles of Sodankylä (altitude 179 m). None of them shows ground influence. This is not to say that this is not possible. Surely, if we would inspect all the profiles we have, we would find dry profiles with ground influence. But this would be a massive undertaking and is out of the scope of the present paper.

Lindenberg is at 0.09 km, and the plotted weighting functions stop there. This is hardly visible in the plot where 2 km altitude difference reduce to about 1 cm (i.e. 100 m translates into about 0.5 mm.

2.14/Section 4.1–4.2/Figure 6–7

My role here is to review the current paper and not the GE17 paper, but the reasoning is both incoherent and irrelevant. The authors argue why a regression line for a UTH difference should be expected to be positive. That may be, and is equivalent to stating the regression line for a UTH

y vs x is expected to be larger than one. Whether one plots y vs x or y-x vs x makes no difference to this reasoning. And then the GE17 reasoning does not even apply for the present paper, because here the quantity is in brightness temperature, not UTH, and the authors already point out the slope is 1 and intercept near 0. So, their GE17 reply is both incoherent and irrelevant.

In figures 2, 3, and 5, the authors plot y-x vs x. They should do the same for figures 6 and 7. This will make it much easier to read. As currently presented, it is hard to tell the range of y-values where the x-value is 240 K.

We have plotted the y-x vs x plots as requested. We have added them in Figures 6 and 7 and have included corresponding text at the end of sections 4.1 and 4.2.

2.16/Section 5.2

I disagree that uncertainty estimates are not required to conclude that numbers are similar. Evidently the authors have calculated those uncertainties, so it should be easy to add them, along with a note of how they were calculated. With the estimated uncertainties, there is a significant difference between the GE17 estimate and the present estimate. This should be admitted and commented upon. I suspect the uncertainties in both cases are underestimated due to the use of a simple linear regression, and that a more sophisticated form of regression such as error-in-variables models would be required to get realistic uncertainties. If two independent estimates (GE17 and the present) of the same value differ by more than one would expect from their uncertainties, then either the estimates or their uncertainties are inconsistent/incomplete. There are almost certainly good reasons that the estimates are different, so what this shows is that the uncertainty from the linear regression underestimates the actual uncertainty on the parameters, which includes many other aspects. I don't expect that the authors go through the effort of a complete uncertainty calculation, as this is a major undertaking. However, I do think the authors need to comment that the two estimates differ by more than their uncertainty and that additional work would be needed to determine the cause.

The fit coefficients and 1-σ uncertainties from Eq. 4 are

$$a = 47.72 \pm 0.14, \qquad b = 0.8025 \pm 0.0006$$

. These coefficients have been determined using the **fit** function of gnuplot, which in turn uses a nonlinear least-squares Marquardt-Levenberg algorithm (Press, 1989, ch. 14.4). In this calculation we have not used uncertainties for $T_{12/14}$ and all values get the same weight. This requires that the computed uncertainties have to be multiplied by $\sqrt{\chi^2/\mathrm{dof}}$ which is 2.3 in our case. Thus, the 1-σ uncertainties, accounting for this kind of error, become 0.32 for a and 0.001 for b, which is still very small. These latter uncertainties will be given in the new version of the paper.

The referee is probably right in supposing that these uncertainties are still quite underestimated. Evidence for this conjecture is provided by comparison of the coefficients of the linear least squares fit from above with the coefficients of the bivariate regression given in the paper. The bivariate regression corrects for regression dilution that happens when errors in the regressor (i.e. $\hat{T}_{12/15}$) are not accounted for. The difference between the slope coefficients of the ordinary and bivariate regression is considerably larger than the error estimates given above (i.e. 0.8025 vs. 0.9256). If we take this difference as a measure of uncertainty of the slope parameter, then the differences between the present parameters and those in GE17 (i.e. 0.8025 vs. 0.8290 for the OLS and 0.9256 vs. 0.994 for the bivariate regression) are relatively small. At least in this sense one may state that the present Figure 9 is similar to the corresponding Figure 2 in GE17.

The new text in section 5.2 will present these considerations.

2.18/Figure 6

My comment on "modest and unsurprising" referred to my conclusion from your results, which was that it is impossible to produce a homogeneous data series (I think there is no need for sarcastic remarks in the response to reviewers). If the authors were to show that the results using two independent methods were consistent within traceable uncertainty estimates, which I don't believe they have, that would be more impressive. But thank you for drawing a less strong conclusion, that addresses the main objection I had to the paper in its previous form.

We thank the reviewer for this clarification. Our understanding of "modest and unsurprising" was that the reviewer considered our calculations unnecessary since the results could be known in advance. The question is, however, not whether it is possible to produce a homogeneous time series but whether the statistical correction by Shi and Bates was trustworthy, given that a statistical approach ignores the physics behind the situation. Our paper provides some of this radiation physics. It shows for the first time how characteristics of individual humidity profiles control the ΔT_{12}. We believe our results corroborate the results obtained by Shi and Bates, which is good.

2.23/Figure 4

It has improved but I still think it's hard to tell what's going on. The authors may want to experiment a bit more with lines that are thinner yet but perhaps the nature of the data simply does not allow for a visualisation that can be followed.

These figures have been produced with gnuplot (see http://www.gnuplot.info/), using a default linewidth. I tried to make the lines thinner using lw 0.5 and lw 0.1. The result was the same. It seems that thinner lines than lw 1 are not possible in gnuplot (or my viewing program, ghostview, does not show thinner lines?). Usually, I use thicker lines (lw 3) to get something that can easily be seen in the plots, as in Figure 8.

I think it would be useful to add a note to Section 3 of the paper that relative humidities are reported as integers, as this explains the substantial digitisation seen in the figures.

Agreed and done.

2.25/Figure 8

I believe averaging kernel shows the derivative of the retrieved parameter to the true parameter, whereas the weighting function or Jacobian is the derivative of the retrieved parameter to the measured quantity.

It seems useful to provide some thoughts on the notions weighting function, weighting kernel, and Jacobian.

The solution of the radiative transfer equation in a simple setting is

$$I = I_0\mathcal{T}(0) + \int_0^\infty B(z)\frac{d\,\mathcal{T}(z)}{d\,z}\,d\,z =: I_0\mathcal{T}(0) + \int_0^\infty B(z)\,W(z)\,d\,z,$$

that is, the weighting function is $W = d\,\mathcal{T}/d\,z$ (Harries, 1997). Here, B is the Planck function, $\mathcal{T}$ is transmission, z is altitude and $z = 0$ refers to the ground. If the quantity of interest is the radiant intensity I, or equivalently, the brightness temperature, then W is the weighing function (or weighting kernel) that we need. This is the function, for which we use a generic form in the manuscript and which we plotted in the first reply (note that $d\mathcal{T}/dz = \chi\mathcal{T}$, where χ is the extinction coefficient).

Jackson and Bates (2001) use the same type of solution of the RT equation (without the surface term), using pressure or log pressure as the vertical coordinate. But they call $d\mathcal{T}/d\ln p$

simply the transmission function. In their paper the word "weighting" is reserved for something different. They use the retrieval formula by Soden and Bretherton (1993), in inverse form:

$$a + bT_{12} = \ln\left(\frac{\langle RH\rangle P_0}{\beta\cos\theta}\right).$$

This equation contains two averages, $\langle RH\rangle$, and $\beta = \langle d\ln T/d\ln p\rangle$. Jackson and Bates study how different formulations of these averages using two different *weighting functions* affect the scatter of the results. One of these weighting functions is given as fixed weights from their table 1, the other is, according to a suggestion in Stephens et al. 1996, the transmission weighting function from above, that is $d\mathcal{T}/d\ln p$.

Neither Harries nor Jackson and Bates use Jacobians. The latter are derivatives of the brightness temperature to any factor influencing it, in our case it would be $dT_{12}/dRH(z)$. Of course this can also be considered as a kind of weighting function, but to our view it would more properly be considered a sensitivity profile or function of influence.

The interpretation (i.e. meaning) of $W(z)$ differs from that of the Jacobian. As said, $dT_{12}/dRH(z)$ gives the change of brightness temperature for a change of RH in a certain altitude, while $W(z)$ measures the contribution of photons emitted at z to the signal that reaches the satellite. Eventually, $\mathcal{T}(z)$ is a function of $RH(z)$ (more correctly, a functional: at each z, $\mathcal{T}(z)$ is a function of the complete RH profile from z to the top of the atmosphere). Thus, the weighting function $W(z)$, since it depends on RH and other quantities (temperature, gas concentrations, ...) is more general than Jacobians. Both quantities are useful, but probably to different degrees in different applications.

For individual profiles $\mathcal{T}(z)$ and $RH(z)$, the information contained in individual weighting functions and Jacobians is confined to the respective profile. While we know an expression for a generic weighting profile, we don't know one for a generic Jacobian, and in fact we doubt that one could be derived. Thus it is necessary and justified for our argumentation to use generic weighing functions.

References

Harries, J.E.: Atmospheric radiation and atmospheric humidity. Q.J.R. Meteorol. Soc., 123, 2171-2186.

Press, W.H., Flannery, B.P., Teukolsky, S.A., and Vetterling, W.T.: Numerical recipes, Cambridge University Press, 1989, 702 pp.

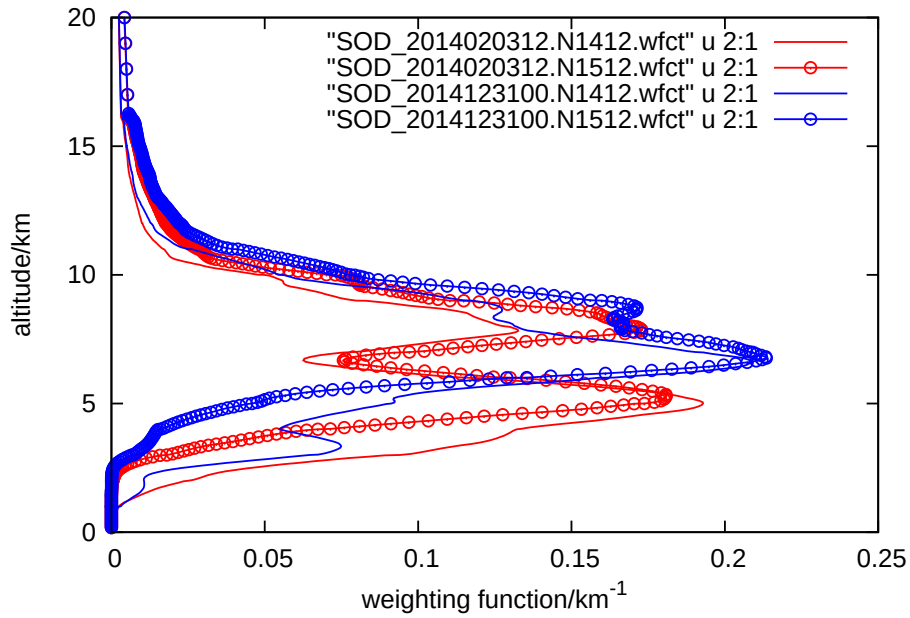

Figure 1: Actual channel 12 weighting functions for NOAA 14 (simple lines) and NOAA 15 (lines with circles) for two winter radiosonde profiles from Sodankylä (dates given).

Intercalibration between HIRS/2 and HIRS/3 channel 12 based on physical considerations

Klaus Gierens[1], Kostas Eleftheratos[2], and Robert Sausen[1]

[1]Deutsches Zentrum für Luft- und Raumfahrt, Institut für Physik der Atmosphäre, Oberpfaffenhofen, Germany

[2]Department of Geology and Geoenvironment, National and Kapodistrian University of Athens, Athens, Greece

Correspondence to: Klaus Gierens (klaus.gierens@dlr.de)

Abstract. HIRS brightness temperatures at channel 12 (T_{12}) can be used to assess the water vapour content of the upper troposphere. The transition from HIRS/2 to HIRS/3 in 1999 involved a shift in the central wavelength of channel 12 from $6.7\,\mu\mathrm{m}$ to $6.5\,\mu\mathrm{m}$ causing a discontinuity in the time series of T_{12}. To understand the impact of this change in the measured brightness temperatures, we have performed radiative transfer calculations for channel 12 of HIRS/2 and HIRS/3 instruments, using a large set of radiosonde profiles of temperature and relative humidity from three different sites. Other possible changes within the instrument, apart from the changed spectral response funtion, have been assumed to be of minor importance and in fact, it was necessary to assume as a working hypothesis that the spectral and radiometric calibration of the two instruments did not change during the relatively short period of their common operation. For each radiosonde profile we performed two radiative transfer calculations, one using the HIRS/2 channel response function of NOAA 14 and one using the HIRS/3 channel response function of NOAA 15, resulting in negative differences of T_{12} (denoted as $\Delta T_{12} := T_{12/15} - T_{12/14}$) ranging between $-12\,\mathrm{K}$ and $-2\,\mathrm{K}$. Inspection of individual profiles for large, medium and small values of ΔT_{12} pointed to the role of the middle tropospheric humidity. This guided us to investigate the relation between ΔT_{12} and the channel 11 brightness temperatures which are typically used to detect signals from the middle troposphere. This allowed us to construct a correction for the HIRS/3 T_{12}, a correction that leads to a pseudochannel 12 brightness temperature such as if a HIRS/2 instrument had measured it. By applying this correction we find an excellent agreement between the original HIRS/2 T_{12} and the HIRS/3 data inferred from the correction method with $R = 0.986$. Upper tropospheric humidity (UTH) derived from the pseudoHIRS/2 T_{12} data compared well with that calculated from intersatellite-calibrated data, providing independent justification for using the two intercalibrated time series (HIRS/2 and HIRS/3) as a continuous HIRS time series for long term UTH analyses.

1 Introduction

Climate variability studies require the analysis of long homogeneous time series of climate data. E.g., a long time series to study the variability of upper–tropospheric water vapour can be derived from the brightness temperature measurements of the

High–Resolution Infrared Radiation Sounder (HIRS) instrument aboard the National Oceanic and Atmospheric Administration (NOAA) polar orbiting satellites. The HIRS measurements started in mid–1979 and are still ongoing. They provide a unique long–term data set (covering nearly 4 decades) that can be exploited in climate research. When NOAA launched the weather satellite NOAA 15 in 1998, it was equipped like all its precursors with a HIRS instrument. This 20–channel instrument provides information of temperature and humidity in the troposphere, where channels 10 to 12 are sensitive to water vapour in different altitude bands (lower to upper troposphere, Soden and Bretherton, 1996). Unfortunately, with the launch of NOAA 15 the central frequency in channel 12 has moved from $6.7\,\mu\mathrm{m}$ to $6.5\,\mu\mathrm{m}$. This is quite a large change, because it means that the channel has its maximum sensitivity about $1\,\mathrm{km}$ higher (and accordingly several degrees colder) than channel 12 of all previous satellites.

With that change, i.e. the transition from HIRS/2 on the older NOAA satellites to HIRS/3 on NOAA 15, the channel 12 time series became inhomogeneous. Shi and Bates (2011) performed an intercalibration, based on statistics of differences between the brightness temperatures measured by subsequent HIRS instruments (technically a regression of first kind). The intercalibration solved the problem of a broken time series for some of the statistics of the data, e.g. for the mean values. The intercalibrated time series was used for several studies (e.g. Gierens et al., 2014; Chung et al., 2016). Yet problems remained in the lower tail of the distribution of brightness temperatures, that is, at the lowest values of brightness temperatures, as has been detected by Gierens and Eleftheratos (2017, in the following cited as GE17).

However, the question arises whether it is sufficient to solve a physical problem (i.e. the different altitudes of peak sensitivity of the channel 12 on HIRS/2 and HIRS/3) with a purely statistical method. Hence, GE17 posed the following question:

> Is it justified at all to combine all HIRS T_{12} (the brightness temperature measured by channel 12) data into a single time series when it is a matter of fact that HIRS 2 and HIRS 3/4 sense different layers of the upper troposphere, layers that overlap heavily but whose centres are more than one kilometre apart vertically?

In fact, this question can be broken down into sub–questions: (1) Under which circumstances is the Shi and Bates (2011) intercalibration justified or not? (2) Which assumptions have to be made about the structure of temperature and moisture profiles? The present paper deals with such questions. Fortunately it turns out that it is possible and justified to combine the channel 12 time series on physical reasoning providing a homogeneous time series of 35+ years that can be used for climatological studies. In this paper we demonstrate that independent tests, based on results from radiative transfer calculations, lead to a comparison between NOAA 14 and NOAA 15 channel 12 brightness temperatures that is very similar to the same comparison performed with the intercalibrated data from Shi and Bates (2011). For these tests we assume that other potential sources of brightness temperature differences (spectral and radiometric calibration) are of minor importance compared to the effect of radiation physics. With this in mind we may say that our new procedure based on physics of radiative transfer corroborates the statistically based procedure of Shi and Bates (2011) and this is good news.

The present paper is organised as follows. First, the radiative transfer model and its setup is introduced in section 2. Section 3 presents radiative transfer calculations for channel 12 on NOAA 14 and NOAA 15, using radiosonde profiles with high vertical resolution. From these calculations we find that certain profile characteristics in the middle troposphere yield either relatively

small or relatively large differences between the computed channel 12 brightness temperatures. In section 4, HIRS channel 11 radiative transfer calculations are applied to get one piece of information more on these profile characteristics. It turns out that the channel 12 brightness temperature differences are linearly correlated with the channel 11 brightness temperatures. A bilinear regression is performed resulting in a superposition of HIRS/3 channel 11 and 12 brightness temperatures from NOAA 15 that produces a pseudo–channel 12 brightness temperature *as if* it was measured by the HIRS/2 instrument on NOAA 14. A discussion of the method and an application to real HIRS data from NOAA 14 and NOAA 15 are presented in section 5, where we show that the comparison of the original NOAA 14 channel 12 brightness temperature with the pseudo–channel 12 brightness temperature from NOAA 15 is quite similar in its statistical properties to a corresponding comparison using the intercalibrated data. The concluding section 6 summarises the logic of the procedure and gives an outlook.

2 Radiative transfer simulations of channel 12 radiation for HIRS/2 and HIRS/3

In order to analyse the differences between channels 12 of HIRS/2 on NOAA 14 and of HIRS/3 on NOAA 15, respectively, we perform radiative transfer calculations using the channel 12 spectral response functions of the two instruments applied to a large set of atmospheric profiles of temperature and relative humidity. These functions are shown in figure 1. In particular, for each profile we perform two runs of the LibRadtran radiative transfer code (Emde et al., 2016), one for channel 12 on NOAA 14 and one for channel 12 on NOAA 15, i.e., we calculate the channel 12 brightness temperatures $T_{12/15}$ and $T_{12/14}$, which would have been measured by NOAA 15 and NOAA 14, respectively. We then calculate the brightness temperature differences $\Delta T_{12} := T_{12/15} - T_{12/14}$ and analyse how a given difference depends on the given profile characteristics. The channel spectral response functions have been obtained from EUMETSAT's NWP SAF [1].

LibRadtran is used with the following set-up: We use the DISORT radiative transfer solver (Stamnes et al., 1988) with 16 discrete angles and the representative wavelengths band parameterization (reptran, Gasteiger et al., 2014) with fine resolution ($1\,\mathrm{cm}^{-1}$). We assume a ground albedo of zero, **Text deleted** and cloud–free scenes (as brightness temperatures from the Shi and Bates data set are cloud cleared, see Shi and Bates, 2011). The background profiles of the absorbing gases are taken from implemented standard atmosphere profiles (Anderson et al., 1986), whereby the appropriate profile is automatically selected from the geographical position and the time to which the radiosonde profile refers. We calculate the channel–integrated brightness temperatures at top of the atmosphere for nadir and 30°off–nadir directions for these profiles.

The atmospheric profiles of temperature and relative humidity (with respect to liquid water) are taken from large sets of radiosonde data with high vertical resolution: (1) We use the set of profiles from the German weather observatory Lindenberg (52.21° N, 14.12° E, Spichtinger et al., 2003) similar to earlier satellite studies (Gierens et al., 2004; Gierens and Eleftheratos, 2016). We use this set of more than 1500 profiles to derive a regression based solution (our training data set). (2) To see whether there are systematic differences between latitude zones also radiosonde profiles from Sodankylä, Finland (67.37° N, 26.60° E), and Manus, Papua New–Guinea (2.06° S, 146.93° E) are used. These weather observatories belong to the Global

[1] Satellite Application Facility, SAF, for numerical weather prediction, NWP, https://nwpsaf.eu/site/software/rttov/download/coefficients/spectral-response-functions, last access in March 2017

Climate Observing System (GCOS) Reference Upper-Air Network (GRUAN). The data and products of the GRUAN network are quality-controlled as described by Immler et al. (2010); Dirksen et al. (2014). We use one year of profiles from both stations, 2013 for Manus and 2014 for Sodankylä. These profiles were used for testing the regression that we derived from the Lindenberg profiles. **Text deleted** The GRUAN profiles have a very high vertical resolution, too high for the radiative transfer calculation. Thus, only every 10th record has been used from the surface to 90 hPa. At higher altitudes (mainly in the dry stratosphere) we have replaced the radiosonde data by data from the standard atmospheres implemented in LibRadtran.

3 Discussion of radiative transfer results

Figure 2 displays the pseudo channel 12 brightness temperatures for $T_{12/15}$ against the corresponding brightness temperature differences (NOAA 15 minus NOAA 14), ΔT_{12}, computed with LibRadtran for the Sodankylä and the Manus profiles. $T_{12/15}$ and ΔT_{12} are presented for nadir and 30°off–nadir directions. As expected, the brightness temperatures for the two considered viewing directions differ, and their difference is rather constantly about 1 to 2 K. More precisely, the summary statistics for the two locations are: At Sodankylä the mean difference at nadir is -6.7 ± 1.2 K, and the mean difference at 30° is -6.7 ± 1.3 K. At Manus the mean difference at both nadir and at 30° are -7.1 ± 0.9 K. It is thus sufficient to only use the nadir radiances for further analyses. It can be noted that $T_{12/15}$ varies between 225 and 242 K for the Sodankylä profiles, while the corresponding ΔT_{12} ranges between -12 and -3 K. There is no obvious correlation between ΔT_{12} and $T_{12/15}$. For Manus, the data pairs show values of $T_{12/15}$ from roughly 229 to 241 K and brightness temperature differences ranging from -10 to -5 K. Again there is no obvious correlation between the brightness temperatures themselves and the corresponding differences.

Figure 3 (top) displays the corresponding results for the radiosonde profiles from Lindenberg. The data pairs form two groups: a large patch at low $T_{12/15}$ and a "tail" at small ΔT_{12}, but higher $T_{12/15}$. This tail has been discarded from further analysis since inspection of the corresponding profiles showed that the relative humidity sensor was obviously malfunctioning in the middle and upper troposphere (and in the stratosphere), indicating zero relative humidity. 1558 profiles out of the total 1660 profiles remain for the analysis. The bottom part of figure 3 shows the same data, without the mentioned tail, and represented as a 2-d histogram. The data at the maximum frequency (red colours) have a brightness temperature difference of about -7 K. Only a small set of the data pairs have $\Delta T_{12} > -5$ K and an even smaller set has $\Delta T_{12} < -11$ K.

At this point it is useful to recall that the weighting functions of the two considered channels peak in altitudes about 1 km apart because the water vapour optical thickness is larger at the central frequency of channel 12 on HIRS/3 than that on HIRS/2. The vertical distance of 1 km implies an air temperature difference of about 6.5 K on average in the upper troposphere, and this explains that an average ΔT_{12} of about the same value is found in the radiative transfer calculations. A similar (average) correction of 8 K has been derived by Shi and Bates (2011) and used by Chung et al. (2016).

Now the question arises how characteristics of humidity profiles are reflected in the brightness temperature differences. Figure 4 shows three sets of relative humidity profiles: 5 profiles with $\Delta T_{12} < -11$ K (left panel), 6 profiles with $-7.21\,\mathrm{K} < \Delta T_{12} < -7.19\,\mathrm{K}$ (middle), and 20 profiles with a small difference, $\Delta T_{12} > -5$ K (right). Note that relative humidity values are reported as integers in our data set, which explains the somewhat angular structure of some of the profiles.

The first set of profiles with $\Delta T_{12} < -11\,\mathrm{K}$ is characterised by high values of RH in the upper troposphere (200 to 400 hPa) and a very dry middle troposphere (450 to 650 hPa). Accordingly, channel 12 on NOAA 15 (ch. 12/15) gets more radiance from the upper levels than channel 12 on NOAA 14 (ch. 12/14) because it is more sensitive there. In turn, ch. 12/14 cannot balance this deficit in the middle tropospheric levels since it is too dry at this altitude. The result is a large negative difference of brightness temperatures. The profiles with $\Delta T_{12} > -5\,\mathrm{K}$ are in turn characterised by a middle troposphere that has much higher relative humidity than the upper troposphere. Under such a circumstance the peak of the ch. 12/15 weighting function approaches the peak of the ch. 12/14 weighting function, that is, the brightness temperatures become more similar. Finally, an average brightness temperature difference is found for profiles without strong humidity contrast between the upper and the middle tropospheric levels, as shown in the middle panel of Figure 4.

This analysis shows that one can understand from consideration of the underlying radiation physics why the brightness temperature differences sometimes obtain large and sometimes relatively small values, and why the average difference is of the order $-7\,\mathrm{K}$. It is, however, clear that this additional knowledge is not available when satellite data analysis is confined to channel 12 only. To exploit this knowledge one need further pieces of information, in particular on the humidity in the mentioned middle tropospheric levels. Fortunately, this knowledge is available from the same HIRS instruments, from channel 11 (see, e.g., Soden and Bretherton, 1996).

4 Construction of a pseudo HIRS/2 channel 12

4.1 Regression using HIRS/3 channels 11 and 12

HIRS/3 channel 11 is centred at a wavelength of 7.3 µm. While the strong water vapour ν_2 vibration–rotation band has its peak line strenghts at about the channel 12 wavelength ($\approx 6.5\,\mu\mathrm{m}$), channel 11 is centred on the longwave side of this band, off the peak with lower line strengths, and thus channel 11 is characteristic of the water vapour in lower levels than channel 12. In a standard midlatitude summer atmosphere channel 11 peaks at about 5 km altitude (see figure 2 of Gierens and Eleftheratos, 2016).

Using the channel spectral response function for channel 11 on NOAA 15, radiative transfer calculations have been performed for the radiosonde profiles used above. Figure 5 shows for the set of Lindenberg profiles the resulting brightness temperatures, $T_{11/15}$, plotted against the previously computed ΔT_{12}. As expected, $T_{11/15}$ is generally higher than the channel 12 brightness temperatures because it characterises the temperature in the middle troposphere where the channel 11 weighting function peaks. $T_{11/15}$ ranges from 248 to 268 K for the Lindenberg profiles. Figure 5 also shows a linear correlation between ΔT_{12} and $T_{11/15}$, although with a large scatter. The linear Pearson correlation coefficient is -0.68. Its square is 0.46, that is, variations of $T_{11/15}$ represent almost half of the variations in ΔT_{12}. The remaining scatter is not surprising given the tremendous variability of relative humidity profiles. One additional piece of information is clearly insufficient to capture all this variability. Nevertheless, the correlation is clearly visible. We have made use of it to construct a correction to the HIRS/3 measured channel 12 brightness temperatures, a correction that leads to a pseudo–channel 12 brightness temperature such *as if* a HIRS/2 instrument had measured it.

For that purpose we try a bilinear regression [2] of the following kind:

$$\hat{T}_{12/15} = a + bT_{12/15} + cT_{11/15}. \quad (1)$$

Here, $\hat{T}_{12/15}$ is the desired pseudo–channel 12 brightness temperature that is equivalent to a HIRS/2 measurement, in other words the $T_{12/15}$ as it would have been $T_{12/14}$. For the calculation of $T_{12/15}$ only the nadir brightness temperatures have been retained as it seems that the off-nadir directions do not yield differing information. The two data vectors containing the brightness temperatures of channels 11 an 12 are linearly correlated with $R = 0.71$, but they point in different directions, that is, they are not co-linear. Regression thus yields a unique result, namely

$$a = -35.4029\,\mathrm{K}, \quad b = 0.775623, \quad c = 0.370927. \quad (2)$$

The one σ uncertainty estimates of the parameters b, c are both ± 0.01. The corresponding data pairs are shown in figure 6. Slope and intercept of the regression (black line in the top panel) are 1.000 and 2×10^{-4}, respectively, and the linear correlation between the linear superposition of channel 11 and 12 brightness temperatures and that of the pseudo–channel 12 brightness temperature is 0.986. The bottom panel shows the same data, but with the difference between regressand and regressor on the y-axis. Maximum deviations from the zero line are about $+3\,\mathrm{K}$ and $-2\,\mathrm{K}$. Mean and standard deviation of the residuals are $0.0 \pm 0.6\,\mathrm{K}$.

4.2 Test with independent radiosonde profiles

Using the linear superposition of channel 11 and 12 brightness temperatures for the considered atmospheric profiles from the two GRUAN stations, Sodankylä and Manus, leads to the data pairs shown in figure 7. The black diagonal in this figure is not the result of a best fit or a regression, it is $y = x$, plotted to guide the eye in checking the result. The residual means $(T_{12/14} - \hat{T}_{12/15})$ and their standard deviations are $0.3 \pm 1.3\,\mathrm{K}$ for Sodankylä and $-0.4 \pm 1.3\,\mathrm{K}$ for Manus. Again, we see that the regression using just one additional piece of information is not able to provide a complete correction with an average residual of zero. But at least these residuals are much smaller than the original differences between $T_{12/14}$ and $T_{12/15}$ shown in Figure 2. Obviously, the superposition methods works well for these data representing a polar and an equatorial atmosphere, respectively.

5 Discussion

5.1 Superposition of weighting functions

The superposition of channels 11 and 12 is equivalent to a superposition of their weighting functions. Figure 8 gives an example. The weighting functions are generic functions as in Gierens and Eleftheratos (2016), assuming a water vapour scale height of $2\,\mathrm{km}$ and peak altitudes of $8.5\,\mathrm{km}$ for ch. 12/15 (red curve), $7.5\,\mathrm{km}$ for ch. 12/14 (black), and $5\,\mathrm{km}$ for ch. 11/15 (blue). The

[2] The regression has been performed using IDL (Interactive Data Language) routine `REGRESS`.

black curve with circles represents the superposition of channels 11 and 12 on NOAA 15 with the weights b and c derived above. The superposition curve (its upper tail, its peak, and about half of its lower tail) is between the corresponding channel 12 weighting functions. We note here that the superposition weighting function. has some weight at lower altitudes where both channel 12 weighting functions. are already very low. Overall, we see that the superposition method eventually brings the pseudochannel 12 brightness temperature of NOAA 15 closer to the level of the corresponding channel 12 brightness temperature of NOAA 14.

Figure 8 (and actual weighting functions shown in the Supplement Figure S1) shows that there is some possibility that channel 11 sees the ground when the atmosphere is quite dry. In such cases, which might occur at high latitudes, the superposition will not work. High brightness temperatures in both channels 10 and 11 could indicate such an event. **Text deleted** Indeed, the (high-latitude) Sodankylä data show larger scatter in fig. 7 than the (equatorial) data from Manus, which might result from unwanted ground influence at the high-latitude station.

An interesting alternative interpretation of the coefficients resulting from the bilinear regression may derive from the following consideration: It is possible to rewrite Eq. 1 as a weighted mean of three temperatures:

$$\begin{aligned} \hat{T}_{12/15} &= a' T_0 + b T_{12/15} + c T_{11/15}, \qquad \text{with} \\ & a' + b + c = 1. \end{aligned} \tag{3}$$

From this interpretation and Eq. 2 follows $a' = -0.14655$ and it turns out that $T_0 = 241.6\,\mathrm{K}$, which is remarkably close to 240 K, the T_0 used as a reference in the retrieval schemes developed by Soden and Bretherton (1993); Stephens et al. (1996); Jackson and Bates (2001). At the altitude where the channel 12 weighting function peaks the temperature is, on average, close to T_0. The remarkable fact is that the regression results just in this T_0 for the constant part, not anything else, a finding that could not be expected *a priori*.

5.2 Application to real data

For the same set of 1004 days of common operation of NOAA 14 and NOAA 15 as used in GE17, we have compared the channel 12 brightness temperatures, daily averages on a $2.5° \times 2.5°$ grid in the northern midlatitudes, 30° N to 70° N. Differing from the previous paper, we use the original non–intercalibrated brightness temperatures. For NOAA 15 we compute the linear superposition derived above, that is, $\hat{T}_{12,15}$, while for NOAA 14 we use $T_{12,14}$. The 2-d histogram of these data pairs is shown in figure 9. It is remarkable how similar this histogram is to a corresponding one shown as figure 2 in GE17 which displays the intercalibrated data. The ordinary least squares linear fit through the new data pairs (solid line) has the equation:

$$(y/\mathrm{K}) = 47.72 + 0.8025\,(x/\mathrm{K}), \tag{4}$$

with a slightly smaller slope and a slightly larger intercept than in GE17 using the intercalibrated data pairs (0.8290 and 41.63, respectively). These coefficients have been determined using a nonlinear least-squares Marquardt-Levenberg algorithm (Press et al., 1989, ch. 14.4). The slope has a 1-σ uncertainty of 0.001. Because the linear least squares fit suffers from regression dilution when errors of the regressor ($\hat{T}_{12,15}$) are not taken into account, we also compute the bivariate regression

(dash-dotted), which has the equation:

$$(y/\mathrm{K}) = 18.24 + 0.9256\,(x/\mathrm{K}), \tag{5}$$

and this has as well a slightly smaller slope and larger intercept than the corresponding fit through the intercalibrated data (which has 0.994 and 2.007, respectively). As such the quoted uncertainty of the slope coefficient (0.001) refers only to the ordinary least squares fit. The difference between the slope coefficients of the ordinary and bivariate regression is considerably larger than the error estimate given above (i.e. 0.8025 vs. 0.9256). If we take this difference as a measure of uncertainty of the slope parameter, then the differences between the present parameters and those in GE17 (i.e. 0.8025 vs. 0.8290 for the ordinary least squares and 0.9256 vs. 0.994 for the bivariate regression) are relatively small. In this sense we may state that **Text deleted** this comparison shows remarkably that two essentially different methods to treat the HIRS 2 to HIRS 3 transition lead to very similar results.

In pursuit of the goal to study changes of upper tropospheric humidity with respect to ice (UTHi) we applied the retrieval formula of Jackson and Bates (2001) to $\hat{T}_{12,15}$ and to $T_{12,14}$ of the common 1004 days. A density plot of the corresponding data pairs of UTHi is displayed in figure 10. Obviously the result is not satisfying; the plot resembles closely the corresponding scatter of data pairs produced from the intercalibrated data (Shi and Bates, 2011) that has been shown in figure 1 of GE17. Unfortunately the superposition method does not solve the problem of a considerable overestimation of the number of super-saturation events recorded with HIRS 3 and 4 instruments and it seems that the pseudo–channel 12 data have to be treated with the cdf–matching technique developed by GE17 in the same way as the intercalibrated data. This is beyond the scope of the present paper.

The new method is an independent approach to an intercalibrated HIRS channel 12 data set, based on results of radiative transfer calculations, classification of profile characteristics and a superposition with information delivered by channel 11. The intercalibration of Shi and Bates (2011) is instead based on pixelwise direct corrections, where the brightness temperature dependent corrections are determined from regressions of the first kind between subsequent satellite pairs. As figures 9,10 show, both methods seem to produce very similar results. **Original text deleted and replaced by:** The statistically based method of Shi and Bates (2011) is thus supported by an independent method, and results obtained from data intercalibrated with either method should be more trustworthy. We thus consider our question from the beginning, whether combining HIRS 2 and HIRS 3 data into a single time series is justified, answered positively. Although both methods produce similar results as we see in fig. 10, neither way of intercalibration solves the problems with the discrepancy in the range of high UTHi values which results from a corresponding discrepancy at the low tail of channel 12 brightness temperatures (see GE17). It is probable that this problem does not originate from the intercalibration procedure, since for the radiative transfer calculation it makes no difference whether the humidity profile contains a very humid upper troposphere with supersaturated layers or not. In each case it provides the corresponding brightness temperature. It is more probable that the problem with the lower tail of the T_{12}-distribution comes from the retrieval method which is based on linearisations around certain "tangential points", thermodynamic properties typical of the upper troposphere (e.g. the $T_0 = 240\,\mathrm{K}$ mentioned above), and that this linear approach is not completely sufficient in cases where actual properties are too far away from the tangential points.

6 Conclusions

The procedure we have developed in the present paper proceeds along the following steps:

1. The difference, $T_{12/15} - T_{12/14} =: \Delta T_{12}$, calculated with LibRadtran for a set of radiosonde profiles, ranges from -12 to $-4\,\mathrm{K}$, with most cases around $-7\,\mathrm{K}$, which fits to the approximately $1\,\mathrm{km}$ altitude difference between the peaks of the channel 12 weighting functions of HIRS/2 and HIRS/3.
2. It turns out that the shape of the RH profile determines whether ΔT_{12} is close to one of the extremes or close to the average. It is particularly the shape of the humidity profile in the lower to middle troposphere that plays a role here.
3. Take channel 11 brightness temperatures as a proxy of that part of the profile, as that channel measures the humidity in the lower to middle troposphere.
4. Indeed, and fortunately, $T_{11/15}$ is correlated to ΔT_{12}; thus it can be used to identify in which cases ΔT_{12} is large, average, or small.
5. Thus it is possible to find a correction to $T_{12/15}$ such that the result is close to (with a mean residual difference of about 1 K) the brightness temperature that N14 would have measured if it had seen the same scene. This correction is a linear superposition of $T_{12/15}$ and $T_{11/15}$, measured by the same HIRS instrument.

Application of this superposition method to real data of 1004 common days of operation of NOAA 14 and NOAA 15, comparing $T_{12/14}$ with the pseudochannel 12 brightness temperature of NOAA 15, $\hat{T}_{12/15}$, yields a 2-d distribution that is very similar to the corresponding distribution obtained with the intercalibrated brightness temperatures by Shi and Bates (2011). Comparing the corresponding values of UTHi again yields a 2-d distribution very similar to that obtained from the intercalibrated data. From these findings we conclude that our method, which is based on radiative transfer calculations, i.e. physics, produces very similar results with Shi and Bates' statistical intercalibration method. The justification to use the intercalibrated channel 12 time series including its early HIRS 2 and later HIRS 3 and 4 phases is thus corroborated. **Old text deleted.**

Note, that this paper shows only the principle of method, how a pseudo HIRS/2 channel 12 brightness temperature can be computed from later HIRS versions, involving channels 11 and 12. As all HIRS instruments have slightly different channel spectral response functions, the regression parameters (a, b, c) will differ from one instrument pair to the other. They will also depend on which HIRS/2 instrument serves as reference. In this paper we used HIRS/2 on NOAA 14, but it certainly makes sense to additionally use HIRS/2 on NOAA 12 as Shi and Bates (2011) based their intercalibration on that satellite. This work is beyond the scope of the current paper and left for future exercise. We note also that this analysis represents a relatively short period in the lifetime of two HIRS instruments, and that their spectral and radiometric calibration was assumed to be constant over this period.

7 Code availability

The libRadtran radiative transfer software package is freely available under the GNU General Public License from http://www.libradtran.org/d

8 Data availability

The GRUAN radiosonde data are available from the GRUAN websites. The special Lindenberg radiosonde data set is available from the first author on request. The NOAA satellite data are available from NOAA public websites.

Author contributions. KG made the radiative transfer calculations and the analyses. KG and RS discussed the procedures and the statistical methods. KE prepared the satellite data in a useful form. All authors contributed to the text.

Competing interests. The authors declare no competing interests.

Acknowledgements. The authors thank the LibRadtran developer team for providing the radiative transfer code and Luca Bugliaro for checking the first author's setup of the radiative transfer job. We are grateful to all the people who provided the data used in this paper, which are colleagues from NOAA, the GRUAN network, and DWD. Christoph Kiemle read the pre-final version of the manuscript and made good suggestions for improvement and further discussion. Thanks for this!

References

Anderson, G., Clough, Kneizys, F., Chetwynd, J., and Shettle, E.: AFGL atmospheric constituent profiles (0–120 km), Tech. Rep. Tech. Rep. AFGL-TR-86-0110, Air Force Geophys. Lab., Hanscom Air Force Base, Bedford, Mass., 1986.

Chung, E.-S., Soden, B., Huang, X., Shi, L., and John, V.: An assessment of the consistency between satellite measurements of upper tropospheric water vapor, J. Geophys. Res., 121, 2874–2887, doi:10.1002/2015JD024 496, 2016.

Dirksen, R., Sommer, M., Immler, F., Hurst, D., Kivi, R., and Vömel, H.: Reference quality upper–air measurements: GRUAN data processing for the Vaisala RS92 radiosonde, Atmos. Meas. Tech., 7, 4463–4490, 2014.

Emde, C., Buras-Schnel, R., Kylling, A., Mayer, B., Gasteiger, J., Hamann, U., Kylling, J., Richter, B., Pause, C., Dowling, T., and Bugliaro, L.: The libRadtran software package for radiative transfer calculations (version 2.0.1), Geosci. Model Dev., 9, 1647–1672, 2016.

Gasteiger, J., Emde, C., Mayer, B., Buehler, S., and Lemke, O.: Representative wavelengths absorption parameterization applied to satellite channels and spectral bands, J. Quant. Spectrosc. Radiat. Transfer, 148, 99–115, 2014.

Gierens, K. and Eleftheratos, K.: Upper tropospheric humidity changes under constant relative humidity, Atmos. Chem. Phys., 16, 4159–4169, 2016.

Gierens, K. and Eleftheratos, K.: Technical Note: On the intercalibration of HIRS channel 12 brightness temperatures following the transition from HIRS 2 to HIRS 3/4 for ice saturation studies, Atmos. Meas. Tech., 10, 681–693, doi:10.5194/amt-2016-289, 2017.

Gierens, K., Kohlhepp, R., Spichtinger, P., and Schroedter-Homscheidt, M.: Ice supersaturation as seen from TOVS, Atmos. Chem. Phys., 4, 539–547, 2004.

Gierens, K., Eleftheratos, K., and Shi, L.: Technical Note: 30 years of HIRS data of upper tropospheric humidity, Atmos. Chem. Phys., 14, 7533–7541, 2014.

Immler, F., Dykema, J., Gardiner, T., D.N. Whiteman, P. T., and Vömel, H.: Reference quality upper-air measurements: guidance for developing GRUAN data products, Atmos. Meas. Tech., 3, 1217–1231, 2010.

Jackson, D. and Bates, J.: Upper tropospheric humidity algorithm assessment, JGR, 106, 32 259–32 270, 2001.

Press, W., Flannery, B., Teukolsky, S., and Vetterling, W.: Numerical recipes, Cambridge University Press, 1989.

Shi, L. and Bates, J.: Three decades of intersatellite–calibrated High–Resolution Infrared Radiation Sounder upper tropospheric water vapor, J. Geophys. Res., 116, D04 108, doi:10.1029/2010JD014 847, 2011.

Soden, B. and Bretherton, F.: Upper tropospheric relative humidity from the GOES 6.7 μm channel: Method and climatology for July 1987, J. Geophys. Res., 98, 16 669–16 688, 1993.

Soden, B. and Bretherton, F.: Interpretation of TOVS water vapor radiances in terms of layer–averaged relative humidities: Method and climatology for the upper, middle, and lower troposphere, J. Geophys. Res., 101, 9333–9343, 1996.

Spichtinger, P., Gierens, K., Leiterer, U., and Dier, H.: Ice supersaturation in the tropopause region over Lindenberg, Germany, Meteorol. Z., 12, 143–156, 2003.

Stamnes, K., Tsay, S.-C., Wiscombe, W., and Jayaweera, K.: Numerically stable algorithm for discrete ordinate method radiative transfer in multiple scattering and emitting layered media, Appl. Optics, 27, 2502–2509, 1988.

Stephens, G., Jackson, D., and Wittmeyer, I.: Global observations of upper–tropospheric water vapor derived from TOVS radiance data, J. Climate, 9, 305–326, 1996.

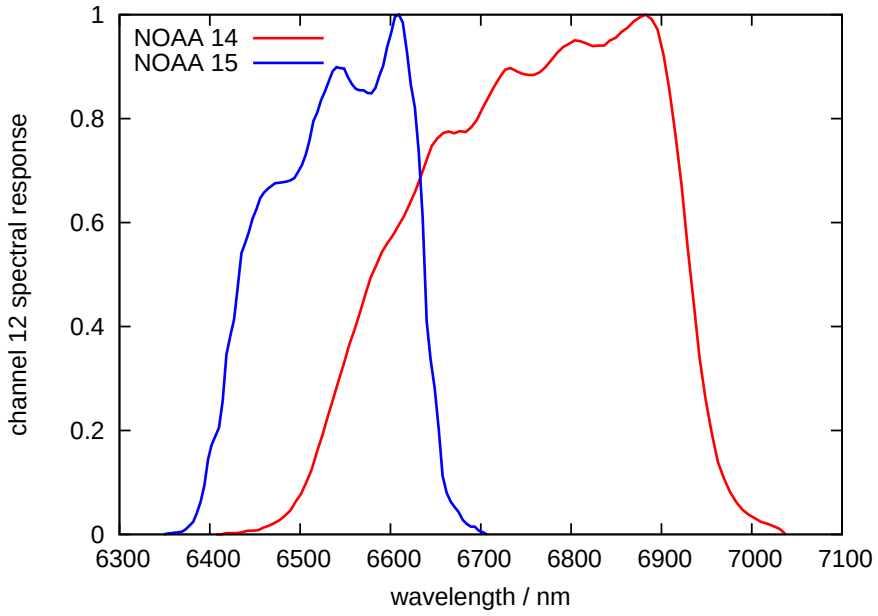

Figure 1. Channel 12 spectral response functions of the HIRS 2 instrument on NOAA 14 and of the HIRS 3 instrument on NOAA 15.

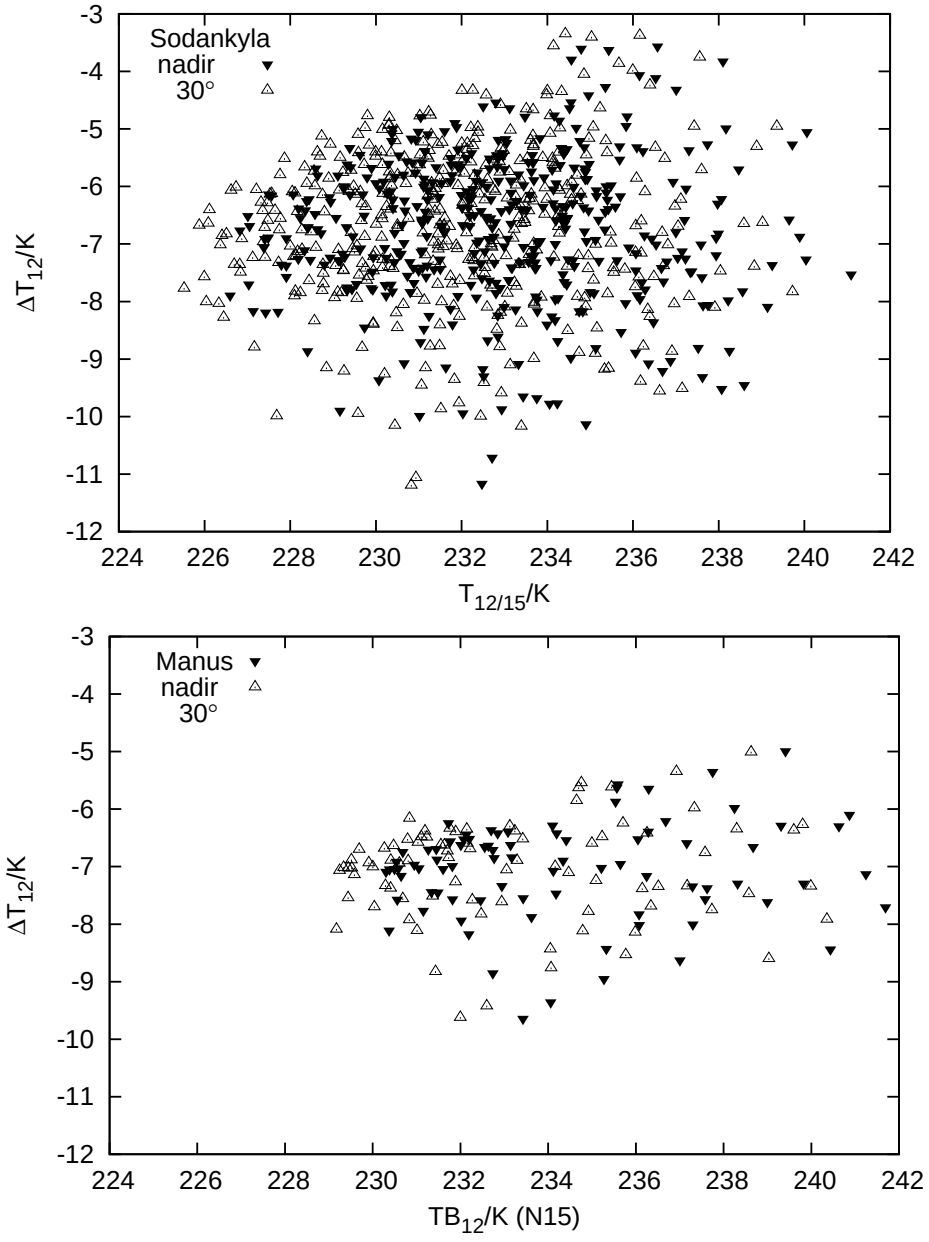

Figure 2. Scatter plot of brightness temperatures calculated with a radiative transfer model using radiosonde profiles from Sodankylä, Finland (top), and Manus, Papua-New Guinea (bottom). The abscissa represents the brightness temperature obtained with a channel 12 spectral response function for HIRS/3 on NOAA 15. The ordinate represents the difference between this brightness temperature and a corresponding one computed using the channel 12 spectral response function for HIRS/2 on NOAA 14. The calculations have been performed for both nadir and 30° off–nadir viewing directions.

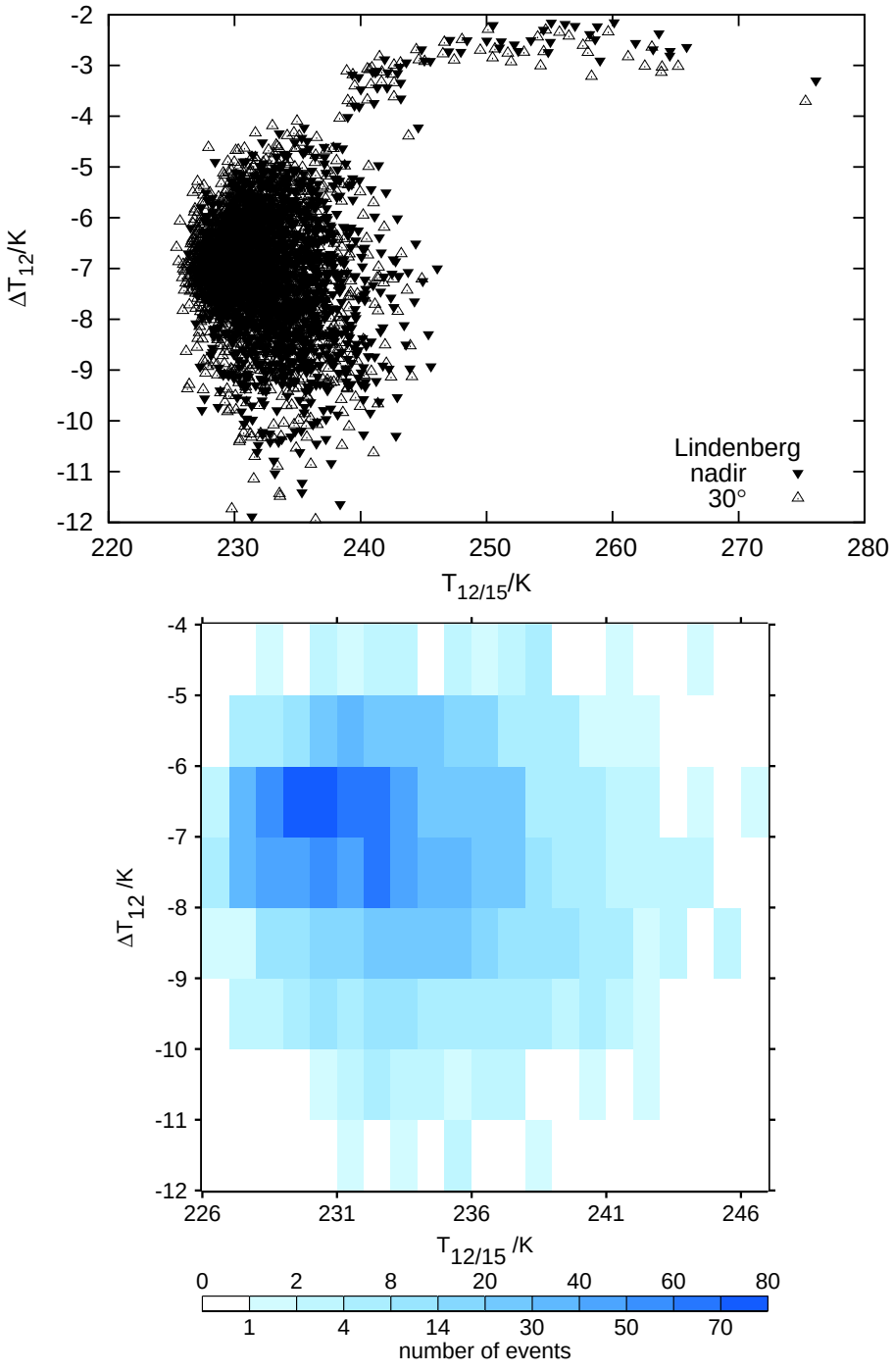

Figure 3. Scatter plot as in figure 2 (top) and a corresponding two–dimensional histogram for channel 12 brightness temperatures computed using radiosonde profiles from Lindenberg, Germany. Note the tail of high values in the scatter plot results from profiles with malfunctioning RH instrument. These 102 profiles have been discarded from further analysis. The 2-d frequency histogram does not contain them anymore. Calculations have been performed for nadir and 30° off-nadir directions, but the off–nadir results are only shown in the scatter plot.

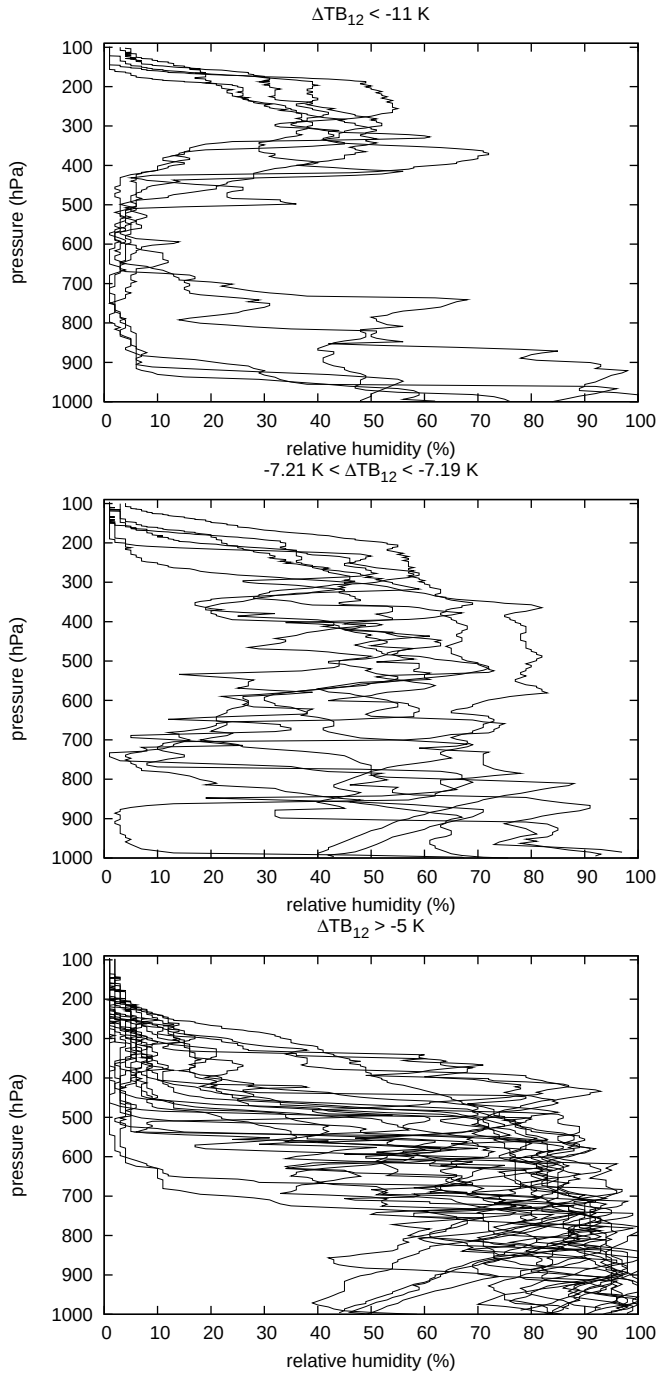

Figure 4. Lindenberg radiosonde profiles of relative humidity vs. pressure altitude that lead to brightness temperature differences in extreme ranges (top and bottom, values indicated in the figures) and to values near to the mean (middle panel). The profiles are obtained from the following launches (format yymmddhh): 00042806, 00122312, 01011506, 01021717, 01030712 (top); 00070112, 00111618, 00112318, 00123012, 01021612, 01040218 (middle); 00021306, 00021312, 00021406, 00022100, 00022106, 00052912, 00053018, 00060706, 00071506, 00080112, 00080200, 00111606, 00121606, 01020118, 01020218, 01022206, 01022218, 01022306, 01022312, 01022400 (bottom).

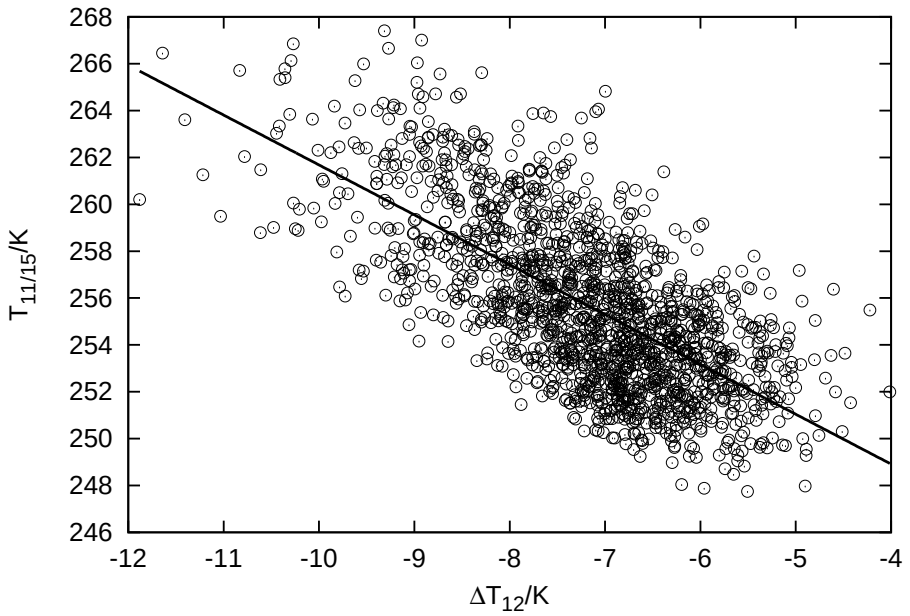

Figure 5. Scatter plot showing a linear correlation between the difference of channel 12 brightness temperatures (NOAA 15 minus NOAA 14) and the NOAA 15 channel 11 brightness temperature computed using the Lindenberg profiles. The linear Pearson correlation coefficient is -0.68.

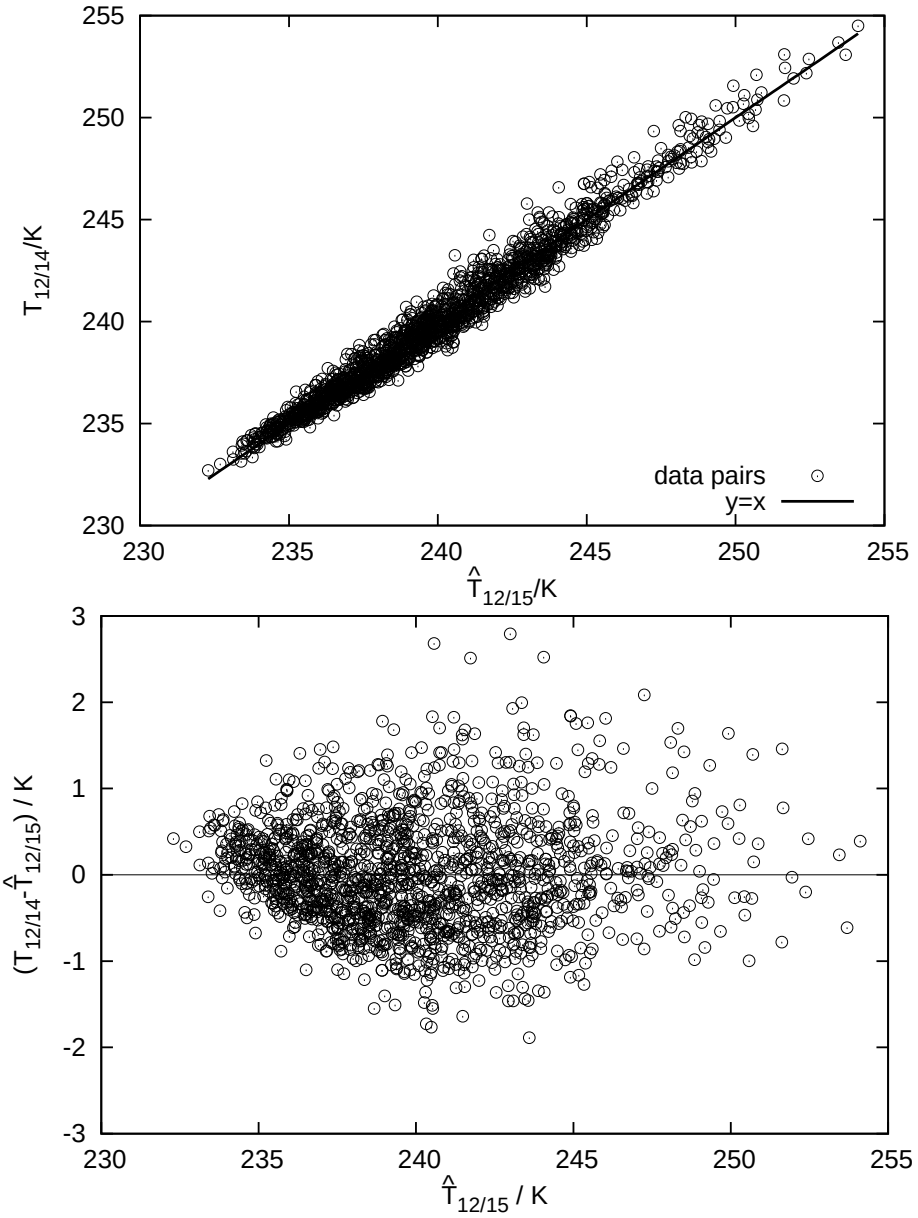

Figure 6. Top: Scatter plot showing a linear correlation between a linear superposition of channel 11 and 12 brightness temperatures from NOAA 15 (abscissa, $\hat{T}_{12/15}$) with the corresponding channel 12 brightness temperature for the same profile but computed with the NOAA 14 channel response function. Note that the fit line has slope 1.000 and the intercept is close to zero (2×10^{-4}). The linear correlation is $R = 0.986$. All data computed using the Lindenberg profiles. Bottom: The same data, plotted with the difference of $T_{12/14} - \hat{T}_{12/15}$ on the y-axis.

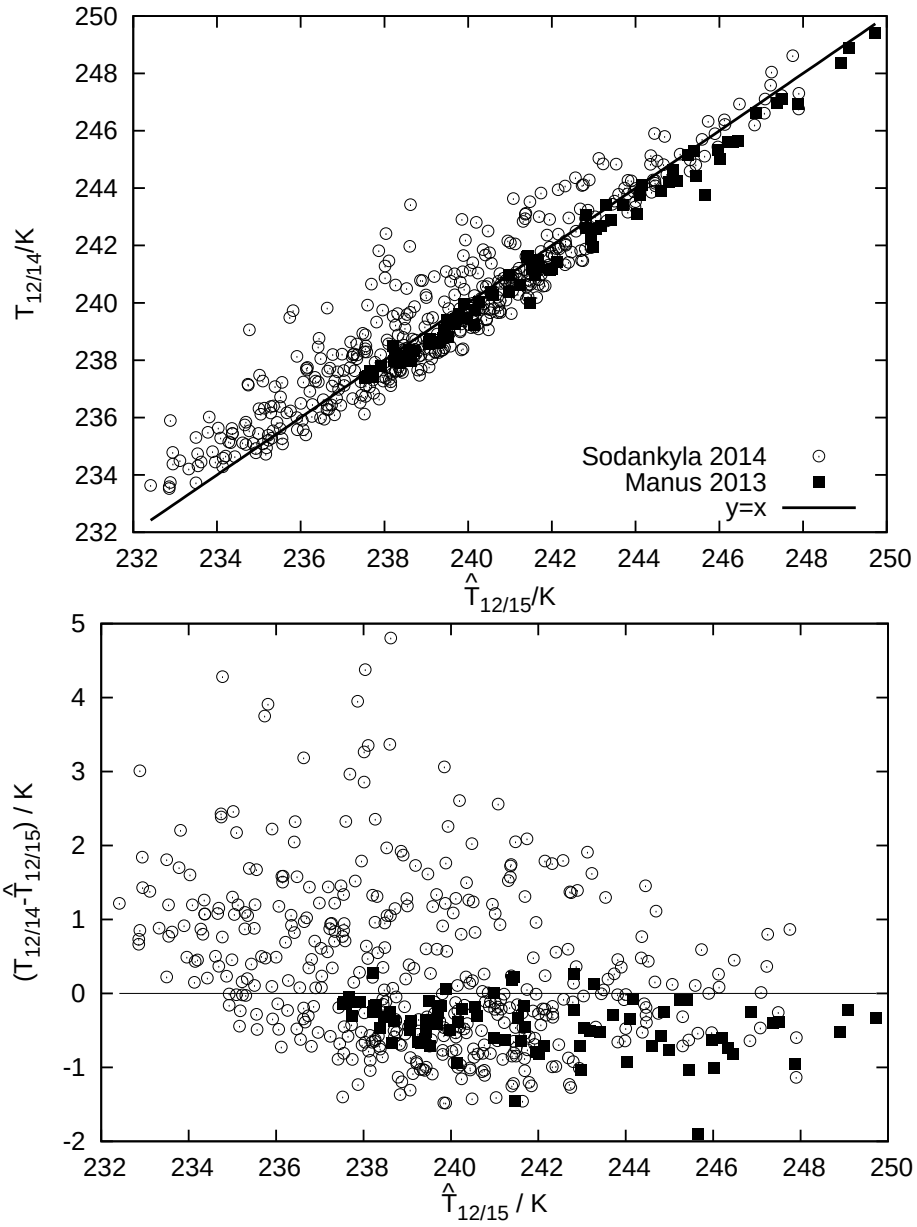

Figure 7. Top: Test of the superposition method using radiosonde profiles from the two GRUAN stations Sodankylä, Finland, and Manus, Papua-New Guinea. The diagonal line ($y = x$) is included to check the result; it is not a fit. Bottom: The same data, plotted with the difference of $T_{12/14} - \hat{T}_{12/15}$ on the y-axis.

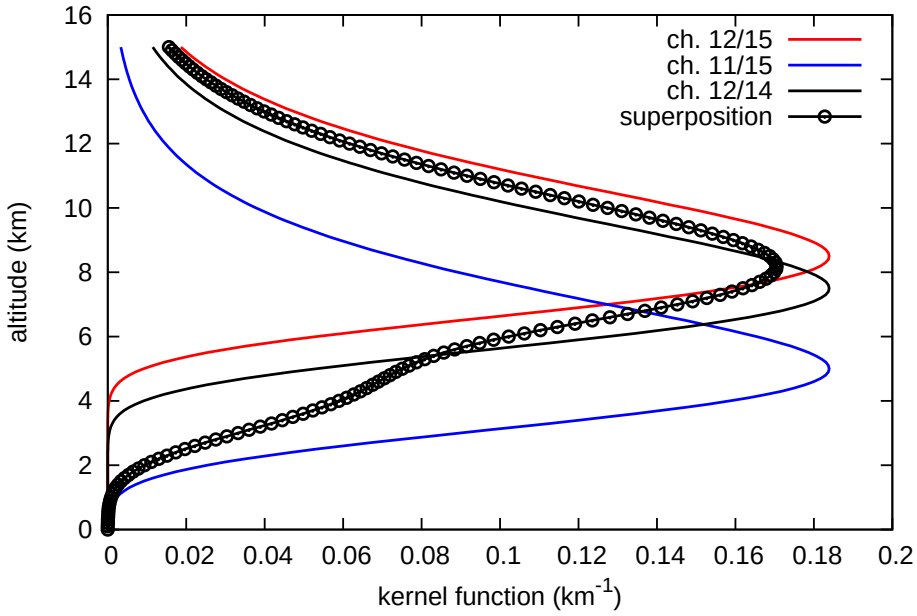

Figure 8. Examples of weighting functions for channels 11 and 12 on NOAA 15 (blue and red), their superposition (black with circles), and channel 12 on NOAA 14 (black).

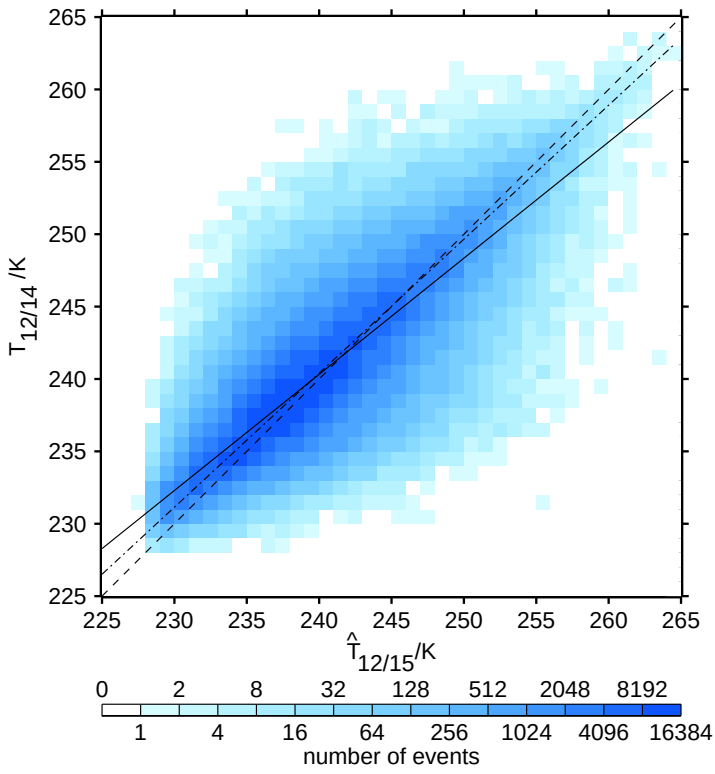

Figure 9. 2–d histogram of brightness temperatures, displaying $\hat{T}_{12/15}$ on the abscissa and $T_{12/14}$ on the ordinate axes, respectively. The data are from 1004 common days of operation of NOAA 14 and NOAA 15. The dashed diagonal line represents $x = y$, the solid line is the best fit according to an ordinary least squares regression and the dashed–dotted line is the bivariate regression line.

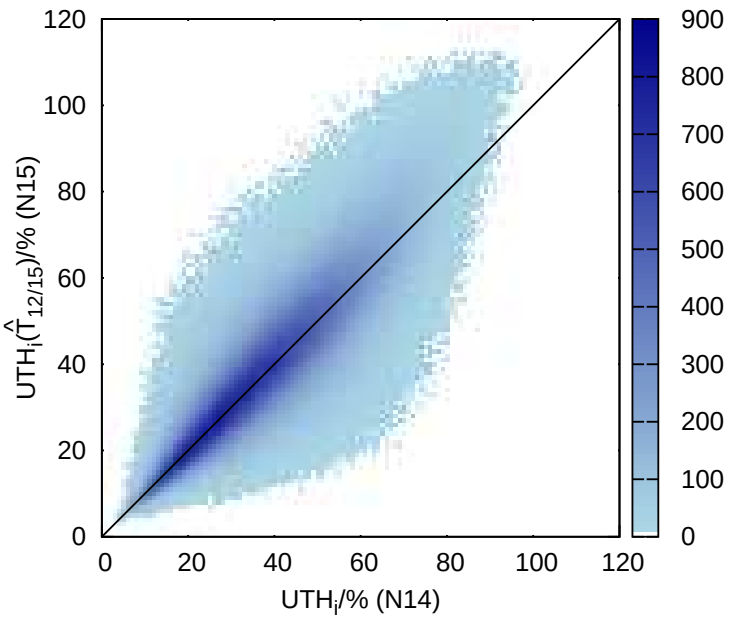

Figure 10. Heat map displaying UTHi computed using $\hat{T}_{12/15}$ on the ordinate against values computed from the original $T_{12/14}$ on the abscissa. Obviously the problem concerning the excess of supersaturation cases in the NOAA 15 data remains even with this new kind of data treatment. The colour scale shows the number of events in each $1\% \times 1\%$ pixel.